NONUNIFORM TARGET IONIZATION AND FITTING THICK TARGET ELECTRON INJECTION SPECTRA TO RHESSI DATA

EDUARD P. KONTAR[1], JOHN C. BROWN[1] and GUILLIAN K. McARTHUR[1,2]

[1]*Astronomy and Astrophysics Group, Dept. of Physics and Astronomy, University of Glasgow, Glasgow G12 8QQ, U.K. (e-mail: john@astro.gla.ac.uk)*
[2]*Catholic University of America, Goddard Space Flight Center*

Abstract. Past analyses of flare hard X-ray (HXR) spectra have largely ignored the effect of nonuniform ionization along the electron paths in the thick-target model, though it is very significant for well-resolved spectra. The inverse problem (photon spectrum to electron injection spectrum $\mathcal{F}_0(E_0)$) is disturbingly non-unique. However, we show that it is relatively simple to allow for the effect in forward fitting of parametric models of $\mathcal{F}_0(E_0)$ and provide an expression to evaluate it for the usual single power-law form of $\mathcal{F}_0(E_0)$. The expression involves the column depth N_* of the transition region in the flare loop as one of the parameters so data fitting can enable derivation of N_* (and its evaporative evolution) as part of the fitting procedure. The fit to RHESSI data on four flares for a single power law $\mathcal{F}_0(E_0)$ is much improved when ionization structure is included compared to when the usual fully ionized approximation is used. This removes the need, in these events at least, to invoke broken power laws, or other forms, of the acceleration spectrum $\mathcal{F}_0(E_0)$ to explain the observed photon spectrum

1. Introduction

To utilize fully the high spectral resolution of RHESSI in diagnosing flare photons and particles, it is essential to correct the observed radiation spectra (already instrument-corrected) for any effects at the Sun which contaminate or distort them. For example, correction for photospheric albedo is discussed elsewhere in this volume (Alexander and Brown, 2002). In the case of thick target model interpretation of hard X-ray (HXR) spectra, one effect, which has been largely ignored in data modeling till now, is that of varying ionization along the thick target beam electron paths. As first discussed by Brown (1973a) the fall of ionization with depth in the atmosphere reduces long-range collisional energy losses and so enhances the HXR bremsstrahlung efficiency there, elevating the high energy end of the HXR spectrum by factors of up to 2.8 above that for an ionized target. The net result is that a power-law electron spectrum of index δ produces a photon spectrum of index $\gamma = \delta - 1$ at low and high energies but with $\gamma < \delta - 1$ in between. The upward knee occurs at fairly low energies, probably masked in data by the tail of the thermal component, while the downward knee occurs in the few deka-keV range, depending on the column depth of the transition zone.

The inverse problem of determining the electron 'injection' spectrum $\mathcal{F}_0(E_0)$ from the HXR spectrum was solved analytically by Brown (1971) for the Bethe-Heitler cross-section, and by Brown and Emslie (1988) for the Kramer's cross-section, and numerically by a variety of approaches (see references in Emslie, Barrett, and Brown, 2001) but only for a uniformly ionized target. Brown *et al.* (1998) finally addressed the inverse problem (using the Kramer's cross-section) for the case of non-uniform ionization and showed the inversion to be not only unstable but non-unique (cf., also Piana *et al.*, 2000). As yet no systematic way to deal with the non-uniqueness has been found, though normal regularisation techniques to deal with the usual instability to noise (Craig and Brown, 1986) do help to suppress it (McArthur, 2000). The mathematical issues involved make this inverse problem rather inaccessible to many users of RHESSI spectral data, despite the fact that the important effect of ionization variation should be included in their modeling to get dependable results. However, many such modelers will be happy to proceed by forward fitting of models of $\mathcal{F}_0(E_0)$ to the HXR spectral data $I(\varepsilon)$ rather than trying to invert the latter to derive $\mathcal{F}_0(E_0)$. This forward approach is satisfactory in that a model of $\mathcal{F}_0(E_0)$ predicts a definite $I(\varepsilon)$ and can be parametrically adjusted to best fit the data (though other $\mathcal{F}_0(E_0)$ may also fit it within the data noise). In this paper we therefore revisit the work of Brown *et al.* (1998), expressing it purely in terms of the forward problem and obtaining expressions we feel will be very useful for thick target modelers of RHESSI data. We also examine whether its inclusion improves the fit to data of photon spectra predicted for single power-law electron injection spectra $\mathcal{F}_0(E_0)$.

2. Thick-Target Spectrum for Nonuniform Target Ionisation

We will denote the electron injection spectrum by $\mathcal{F}_0(E_0)$ (electrons s^{-1} per unit injection energy E_0) and the emitted bremsstrahlung HXR spectrum at the Sun by $I(\varepsilon)$ (photons s^{-1} per unit photon energy ε). Following Brown *et al.* (1998) we treat the electron propagation as 1-D and ignore trapping, relativistic, and directivity effects. The bremsstrahlung cross-section differential in ε,

$$Q(\varepsilon, E) = Q_0 \frac{q(\varepsilon, E)}{\varepsilon E}, \tag{1}$$

yields for the Kramer's approximation $q = 1$

$$J(\varepsilon) = \frac{Q_0}{K'\varepsilon} \int\limits_{\varepsilon}^{\infty} \int\limits_{E}^{\infty} \frac{\mathcal{F}_0(E_0)\, dE_0\, dE}{\lambda + x((E_0^2 - E^2)/2K')}, \tag{2}$$

where $K' = 2\pi e^4 \Lambda$, $\Lambda = \Lambda_{ee} - \Lambda_{eH}$ and $\lambda = \Lambda_{eH}/\Lambda$ (numerically $\Lambda_{ee} = 20$, $\Lambda_{eH} = 7.1$ so $\Lambda = 12.9$ and $\lambda = \lambda_{eH}/\Lambda \simeq 0.55$). $x(M)$ is the atmospheric ionization at the ionization weighted target column density variable M (cm^{-2}) defined in Section 2 of Brown *et al.* (1998).

x changes from 1 to near 0 over a small spatial range on the Sun and the change is even more abrupt in column density range. So, following Brown *et al.* (1998), we approximate $x(M)$ as a step function at depth M_*

$$x(M) = \begin{cases} 1, & M < M_*, \\ 0, & M > M_*, \end{cases} \tag{3}$$

for which Equation (2) becomes, with 'nonuni' denoting non-uniform target,

$$J(\varepsilon)_{\text{nonuni}} = \frac{Q_0}{(\lambda + 1)K'\varepsilon} \int_\varepsilon^\infty \left[\int_E^{(E^2 + 2K'M_*)^{1/2}} \mathcal{F}_0(E_0)\,\mathrm{d}E_0 + \right.$$
$$\left. + \frac{\lambda + 1}{\lambda} \int_{(E^2 + 2K'M_*)^{1/2}}^\infty \mathcal{F}_0(E_0)\,\mathrm{d}E_0 \right] \mathrm{d}E. \tag{4}$$

The limiting case of a uniformly ionized target corresponds to letting $M_* \to \infty$ here or, with "uni" denoting uniform target,

$$J_{\text{uni}}(\varepsilon) = \frac{Q_0}{K\varepsilon} \int_\varepsilon^\infty \int_E^\infty \mathcal{F}_0(E_0)\,\mathrm{d}E_0\,\mathrm{d}E, \tag{5}$$

where $K = 2\pi e^4 \Lambda_{ee}$.

For any model of $\mathcal{F}_0(E_0)$ one wants to test against data, Equation (4) can be used to compute $J(\varepsilon)$ allowing for the nonuniform ionization effect (as compared to Equation (5)) and the parameters of $\mathcal{F}_0(E_0)$ adjusted to find the best fit. Note that in doing so one must either specify the depth M_* of the ionization step (transition region) or regard it as a free parameter to be found as a part of the fitting procedure as was done for *Yokhoh* data by McArthur (2000). This can provide a method of studying changes in M_* due to evaporation as the flare proceeds and, for example, seeing if evolution of M_* is in line with the evaporation rate expected from electron beam heating as first estimated by Brown (1973b) and more precisely studied using various hydrodynamic codes (see, e.g., Aschwanden, 2002).

Note that in the analysis here we have ignored the contribution to the observed $J(\varepsilon)$ of the photospheric albedo $A(\varepsilon)$. The 'reflection' of HXRs in the lower atmosphere leads to a modified observed flux $J_{\text{obs}}(\varepsilon) = J_{\text{flare}}(\varepsilon)(1 + A(\varepsilon))$, where $A(\varepsilon)$ is the integrated reflection coefficient. Note that $A(\varepsilon)$ is somewhat dependent on flare position and as a result should demonstrate center to limb variation, while we are interested in general properties of $J(\varepsilon)$ common to all the flares selected. Moreover, the value of the coefficient A never exceeds about 0.5 so the correction factor is small compared with the ionization effect on energy losses and hence on $J(\varepsilon)$. Therefore, while the effect of albedo should be included in future work, its effect on forward model fitting is less important than ionization for the thick-target

situation. On the other hand, in the problem of inversion of $J(\varepsilon)$ to infer $\mathcal{F}_0(E_0)$ the solution involves derivatives of the albedo $A(\varepsilon)$ as a function of energy and can also be important (Alexander and Brown, 2002).

3. Effect of Ionisation Structure on $J(\varepsilon)$ for Single Power-Law $\mathcal{F}_0(E_0)$

Here we consider the form of $J_{\text{nonuni}}(\varepsilon)$ given by Equation (4) (and also $J_{\text{uni}}(\varepsilon)$ by Equation (5) for comparison) for the commonly used single power-law form of electron injection spectrum $\mathcal{F}_0(E_0)$. In doing so we replace M_* by $E_* = (2K'M_*)^{1/2}$, the transition zone 'stopping energy'.

3.1. POWER-LAW $\mathcal{F}_0(E_0)$

Writing

$$\mathcal{F}_0(E_0) = (\delta - 1)\frac{\mathcal{F}_1}{E_1}(E_0/E_1)^{-\delta} \tag{6}$$

where $\mathcal{F}_1$ is the total injection rate (s^{-1}) above $E_0 = E_1$, results, after one integration, in

$$
\begin{aligned}
J(\varepsilon)_{\text{nonuni}} &= \frac{Q_0\mathcal{F}_1}{(\lambda + 1)K'\varepsilon} \int_\varepsilon^\infty \left[\left(\frac{E}{E_1}\right)^{-\delta+1} + \frac{1}{\lambda}\left(\frac{E^2 + E_*^2}{E_1^2}\right)^{(-\delta+1)/2}\right] \mathrm{d}E \\
&= \frac{Q_0\mathcal{F}_1 E_1}{(\lambda + 1)K'\varepsilon}\left[\frac{1}{\delta - 2}\left(\frac{\varepsilon}{E_1}\right)^{-\delta+2} + \right. \\
&\quad \left. + \frac{1}{2\lambda}\left(\frac{E_*}{E_1}\right)^{(-\delta+2)} B\left(\frac{1}{1 + (\varepsilon/E_*)^2}, \frac{\delta}{2} - 1, \frac{1}{2}\right)\right],
\end{aligned}
\tag{7}
$$

where B is the incomplete beta function,

$$B\left(\frac{1}{1 + (\varepsilon/E_*)^2}, \frac{\delta}{2} - 1, \frac{1}{2}\right) \equiv \int_0^{\frac{1}{1+(\varepsilon/E_*)^2}} x^{\delta/2-2}(1 - x)^{-1/2}\, \mathrm{d}x, \tag{8}$$

and is a well-tabulated function.

For comparison the thick-target photon power law (with $\gamma = \delta - 1$) for the fully ionized target is immediately obtained from Equation (5) (Equation (7) as $E_* \to \infty$),

$$J(\varepsilon)_{\text{uni}} = \frac{Q_0\mathcal{F}_1}{K(\delta - 2)}\left(\frac{\varepsilon}{E_1}\right)^{-\delta+1}. \tag{9}$$
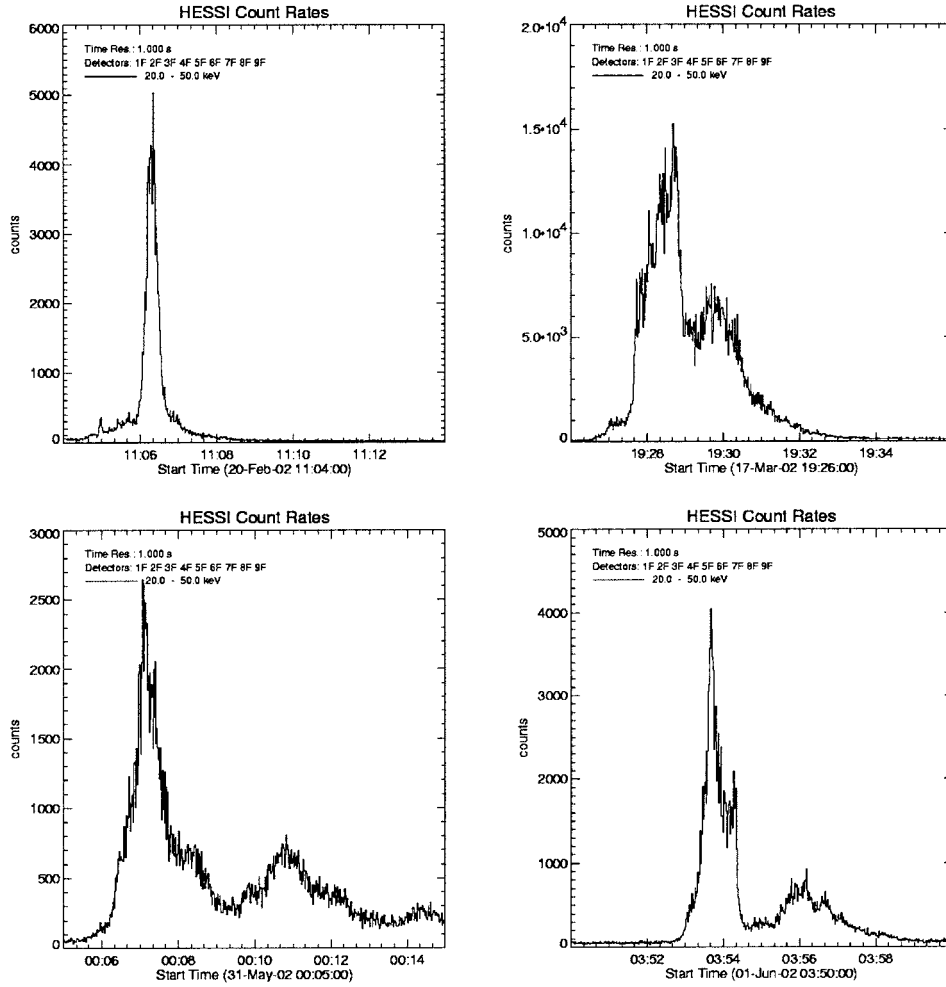
Figure 1. The RHESSI light curves are shown for the low-energy range 20–50 keV, binned in steps of dt_{histo} = 1.0 s. The time intervals taken for the spectral fits are given in Table II.

4. Applications to RHESSI Data

We have chosen four examples of RHESSI flare spectral data sets. These are the events of 20 February at 11:06 UT, 17 March at 19:26 UT, 31 May at 23:52 UT, and 1 June at 00:06 UT. The corresponding light curves are presented in Figure 1 while the locations and classes of the flares are given in Table I. Note that the event of 31 May is very near the limb and if this involves any footpoint occultation our analysis based on the whole thick target source volume may be inappropriate.

TABLE I

Location and flare classification of selected events.

Date	Class	Location	AR
20 Feb. 2002	C7.5	N15 W77	9825
17 Mar. 2002	M4.0	S21 E18	9871
31 May 2002	M2.4	S30 E90	9973
1 June 2002	M1.5	S19 E29	9973

4.1. FULLY IONIZED TARGET WITH SINGLE POWER-LAW $\mathcal{F}_0(E_0)$

After allowance for all instrumental effects (as in Aschwanden, Brown, and Kontar, 2002) the spatially integrated RHESSI spectra in these events can be modeled well as the sum of an isothermal component and a non-thermal component. The energy range below around 10–20 keV (depending on the flare) can be best fit with an exponential function while the range well above this is approximately a power law, though with some steepening at higher energies. The best fit parameter ($\delta = \gamma + 1, kT$) values for a single power law are presented in Table I while the spectral fits, made with the help of SPEX, are shown in Figure 2. The figures clearly show that the greatest deviation from a single power law occurs in the range 30–60 keV (see Figure 2) where the spectra show a downward 'knee'. To improve the fit we need to take a more complex function than the simple power law of Equation (9). This spectral 'knee' in the deka-keV range of ε is often attributed to some sharp feature in $\mathcal{F}_0(E_0)$ such as a broken power law or spectral bump (e.g., Lin and Johns, 1993). However these interpretations are based on the fully ionized target approximation. Here we consider how well the photon data are fit by reverting to a single power law in $\mathcal{F}_0(E_0)$ but allowing for the ionization structure which is certainly present – i.e, by the form predicted in Equation (7).

4.2. NON-UNIFORMLY IONIZED TARGET WITH POWER-LAW $\mathcal{F}_0(E_0)$

We therefore fitted the data with the following model prediction (Equation (7))

$$J(\varepsilon) = \frac{I_0}{(\lambda+1)\varepsilon} \left[\frac{\varepsilon^{-\delta+2}}{\delta-2} + \frac{E_*^{-\delta+2}}{2\lambda} B\left(\frac{1}{1+(\varepsilon/E_*)^2}, \frac{\delta}{2}-1, \frac{1}{2} \right) \right], \qquad (10)$$

where $\lambda = 0.55$ and I_0, E_* and δ are adjustable parameters. Note that I_0 is just a scale factor depending on $\mathcal{F}_0$, E_1 – see Equation (7).

The best-fit results for E_* and δ are presented in Table III, along with the column depth N_* equivalent to E_* and $\chi^2_{\text{nonuni}}/\chi^2_{\text{uni}}$ is the ratio between total χ^2 deviations of the model prediction from the data,
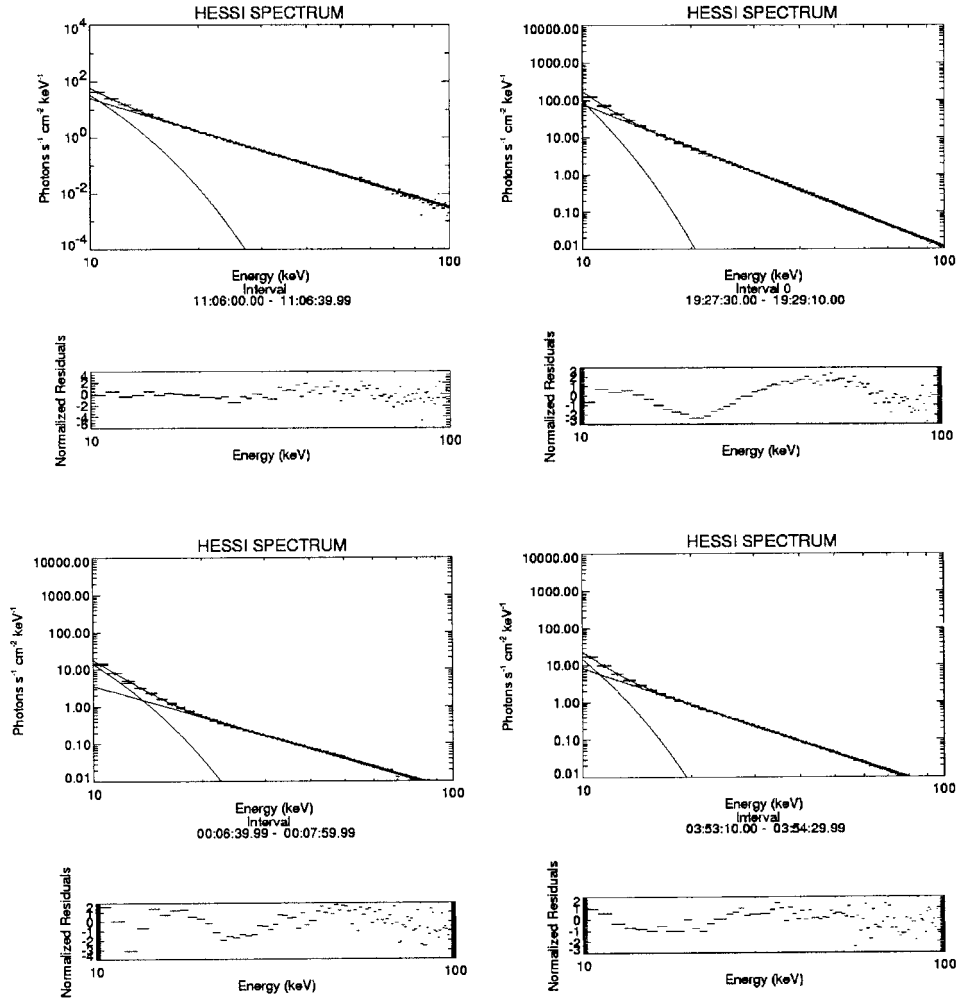
Figure 2. The photon spectra and spectral fits with photon power law plus thermal component in the energy range 10–100 keV (*top panel*). The fit parameters are given in Table II. Normalized residuals are presented in the bottom panel showing the deviation of real data from the power law, $(J_{\mathrm{model}}(\varepsilon) - J_{\mathrm{RHESSI}}(\varepsilon))/J_{\mathrm{RHESSI}}(\varepsilon)$.

$$\chi^2_{\mathrm{model}} = \sum_{i=0}^{N} (J_{\mathrm{model}}(\varepsilon) - J_{\mathrm{RHESSI}}(\varepsilon))^2, \tag{11}$$

for the two models – non-uniformly ($_{\mathrm{nonuni}}$) and uniformly ($_{\mathrm{uni}}$) ionized targets. In the four panels of Figure 3 we show the best-fit spectra superimposed on the data for each of the four events. The overall χ^2 value summed over all data points (11) is much lower for the model allowing for the ionization structure than for the fully ionized case (see Table I) and the individual residuals are also mostly much smaller (note the log scale) in the range 20–60 keV. Above 60 keV the data are pro-

TABLE II

Uniformly ionized target model with single power-law $\mathcal{F}_0(E_0)$ plus thermal component fit for the events – results produced with SPEX.

Date	Time (UT)	δ	kT (keV)
20 Feb. 2002	11:06:00–11:06:40	4.89	1.47
17 Mar. 2002	19:27:30–19:29:10	4.84	1.27
31 May 2002	00:06:40–00:08:00	3.79	2.02
1 June 2002	03:53:10–03:54:30	4.26	1.45

TABLE III

Best fit non-uniformly ionized target model parameters for single power-law $\mathcal{F}_0(E_0)$, and equivalent N_* (energy range 20–100 keV), and the ratio of $\chi^2_{\mathrm{nonuni}}/\chi^2_{\mathrm{uni}}$.

Date	δ	E_* (keV)	N_* (cm^2)	$\chi^2_{\mathrm{nonuni}}/\chi^2_{\mathrm{uni}}$,
20 Feb. 2002	5.29	37.4	2.7×10^{20}	0.032
17 Mar. 2002	4.99	24.4	1.1×10^{20}	0.047
31 May 2002	4.15	56.2	6.1×10^{20}	0.041
1 June 2002	4.46	21.0	8.4×10^{19}	0.055

gressively noise-dominated and therefore both models give similar residuals. Thus, inclusion of the ionization effect allows a much better fit to these RHESSI spectra with a single power-law $\mathcal{F}_0(E_0)$ than does the usual ionized approximation and removes the need to invoke features in the acceleration process producing $\mathcal{F}_0(E_0)$. The inferred best fit δ values are slightly higher in the more realistic ionization model (compare Tables II and III).

4.3. LOCATION OF THE TRANSITION REGION

By assuming that the main spectral feature observed in the HXR spectra is caused by the increased bremsstrahlung efficiency of the chromosphere and not an original feature in the electron spectra, then for a pure power-law $\mathcal{F}_0(E_0)$ the non-thermal part of the HXR spectra can be expressed analytically as the combination of a power law and an incomplete beta function (10). The HXR spectra can be fitted with (10) to determine the three parameters of this model i.e., photon flux constant I_0, electron spectral index δ and the transition zone electron stopping energy E_*.
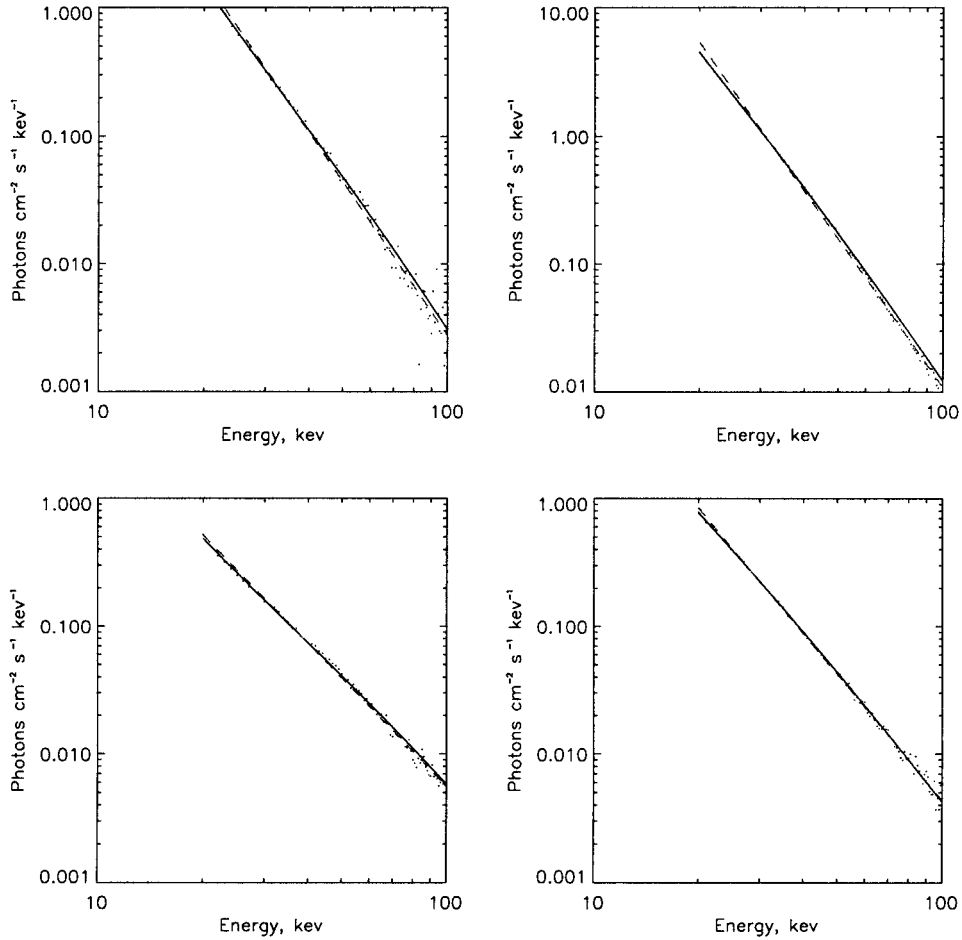
Figure 3. The RHESSI spectra (*dots*) and the spectral fit (cf., Table III) for a non-uniformly ionized target for the 4 selected events. The *solid line* represents the model for the nonuniform fit, *dashed lines* correspond to the single power-law fit.

For these flares, the best fit values of the transition region energy parameter E_* lie in the 20–60 keV range. The stopping energy can be readily converted into a column density of the total material the electron passed through to reach the chromosphere, so this fitting procedure allows estimation of the coronal column density from $E_* = (2K'M_*)^{1/2}$. This corresponds for our events to $M_* = (1.2 - 11) \times 10^{20}$ cm^{-2} with the equivalent N_* in the range $(0.8 - 7) \times 10^{20}$ cm^{-2}. Thus the spectral power of RHESSI enables us to derive the transition region column depth. By extending the work of Aschwanden, Brown, and Kontar (2002) using RHESSI spectral images to derive hard X-ray source heights for limb events and combining this with the spectral estimate of N_* it should be possible to determine the geometric height of the transition region inside the thick target flare loop. This is the subject of a future

paper where we will also attempt to follow the evaporative evolution of N_* as the flare progresses, using our spectral fitting technique.

5. Discussion and Conclusions

Starting from the basic principles of collisional propagation of a thick-target beam in the non-uniformly ionized solar plasma we derived a simple model for its bremsstrahlung spectrum for a general electron injection spectrum $\mathcal{F}(E_0)$. For a pure power-law $\mathcal{F}(E_0)$, with two adjustable parameters $\mathcal{F}_1$, δ plus the stopping energy E_*, we can physically explain the observed deviation from a power-law photon spectrum, agreeing much better with RHESSI data than the pure power law obtained in the usual uniformly ionized target analysis. The method is also transparent and easy to use for general $\mathcal{F}(E_0)$. Finally we note that there are known additional effects which should be included in refined spectral modeling which might lead to deviations from a single photon power law. In particular there is the effect of solar HXR albedo (Alexander and Brown, 2002). In summary, the results show that

– detailed RHESSI spectral data show a deviation from a simple power law in the range 20–100 keV often attributed to a feature in $\mathcal{F}_0(E_0)$, i.e., in the acceleration process.

– inclusion of the effect of target ionization change across the transition region removes the need for any such feature in $\mathcal{F}_0(E_0)$ which can then be a pure power law, favouring a stochastic process.

– using the technique presented in the paper one can determine the energy E_* corresponding to the transition zone depth and hence the value of that column depth.

Acknowledgement

References

Alexander, C. R. and Brown, J. C.: 2002, *Solar Phys.*, this volume.
Aschwanden, M. J.: 2002, *Space Sci. Rev.* (in press).
Aschwanden, M. J., Brown, J. C., and Kontar, E. P.: 2002, *Solar Phys.*, this volume.
Brown, J. C.: 1971, *Solar Phys.* **18**, 489.
Brown, J. C.: 1973a, *Solar Phys.* **28**, 151.
Brown, J. C.: 1973b, *Solar Phys.* **31**, 143.
Brown, J. C. and Emslie, A. G.: 1988, *Astrophys. J.* **331**, 554.
Brown, J. C., McArthur, G. K., Barrett, R. K., McIntosh, S. W., and Emslie, A. G.: 1998, *Solar Phys.* **179**, 379.
Craig, I. J. D. and Brown, J. C.: 1986, *Inverse Problems in Astronomy*, Hilger, Bristol.

Emslie, A.G., Barrett, R.K., and Brown, J.C.: 2001, *Astrophys. J.* **557**, 921.
Lin, R. P. and Johns, C. M.: 1993, *Astrophys. J. Lett.* **417**, L53.
McArthur, G. K.: 2000, PhD Thesis, University of Glasgow.
Piana, M., Barrett, R. K., Brown, J. C., and McIntosh, S. W.: 2000, *Inverse Problems* **15**, 1469.